Annual Methodological Archive Research Review
http://amresearchreview.com/index.php/Journal/about
Volume 3, Issue 10 (2025)

Online ISSN 3007-3197 Print ISSN 3007-3189
http://amresearchreview.com/index.php/Journal/about

Urban Vegetation Cooling Efficiency Along the Urban–Peri-Urban Gradient: A Multi-Temporal Remote Sensing Assessment of Gujranwala, Pakistan

Nouman Akhtar
Centre for Geographical Information System, University of the Punjab, Lahore, Pakistan

Basit Aziz
Centre for Geographical Information System, University of the Punjab, Lahore, Pakistan

Zeeshan Haider
Centre for Geographical Information System, University of the Punjab, Lahore, Pakistan

Prof. Dr Shahid Ghazi
Institute of Geology, University of the Punjab, Lahore, Pakistan

Razi ur Rehman
National University of Sciences & Technology (NUST), Islamabad, Pakistan
Email: razi.urr.rhman@gmail.com

ABSTRACT

Urban vegetation is widely reported to lower land surface temperature (LST), but whether the magnitude of this cooling effect varies with position along the urban–peri-urban gradient, and whether the spatial configuration of vegetation patches matters independently of vegetation amount, remains poorly documented for Pakistani cities. This study examined Gujranwala, Punjab, using Landsat 5, 8, and 9 Collection 2 Level-2 imagery processed in Google Earth Engine across four epochs (2000, 2010, 2020, and 2025). An empirically delineated urban core, based on Dynamic World built-up probability, anchored four concentric distance zones extending to 15 kilometers. LST, NDVI, NDBI, and MNDWI were computed for each epoch and aggregated to a 250-meter grid to limit the inflated statistical significance associated with spatial autocorrelation. NDVI was strongly and negatively associated with LST (coefficient − 16.54, $p < 0.001$, $R^2 = 0.835$), and NDBI was strongly positively associated with LST (coefficient 27.50, $p < 0.001$, $R^2 = 0.871$), consistent with the wider literature. Cooling intensity, defined relative to a local built-up reference temperature, was higher in the urban core and inner-urban zones than in the outer fringe and peri-urban zones in three of the four epochs. Vegetation patch configuration, tested through the Largest Patch Index and patch density, added only a small amount of explanatory power beyond vegetation amount alone (R^2 increase of approximately 0.06 percentage points), with patch contiguity associated with cooling

Online ISSN 3007-3197 Print ISSN 3007-3189

in the expected direction. A systematic, epoch-level offset in mean LST was identified and controlled for using year fixed effects in all regression models. These findings indicate that vegetation amount remains the dominant determinant of surface cooling in Gujranwala, while its spatial arrangement contributes a modest and only partially consistent additional effect.

Keywords: Urban Heat Island; Land Surface Temperature; NDVI; Landscape Configuration; Peri-Urban Gradient

Introduction

Cities are, on average, warmer than the rural land that surrounds them, a difference that has been observed and measured for well over a century and that has grown more pronounced as urban populations and built-up land area have expanded worldwide. This urban heat island effect is not merely a matter of thermal comfort. Elevated surface and air temperatures in cities raise cooling energy demand, worsen air quality, and increase heat-related morbidity and mortality, and these burdens fall disproportionately on residents of rapidly urbanizing, resource-constrained cities that have the least capacity to adapt. Vegetation is consistently identified as one of the few practical, scalable interventions available to city planners for moderating this effect, because plant canopies shade impervious surfaces, evapotranspire, and reduce the net radiation absorbed at the land surface. Understanding precisely how much cooling a given amount of vegetation delivers, and whether that delivery depends on where the vegetation is located within a city, is therefore a question with direct relevance to urban planning and climate adaptation policy, not only to academic land-surface climatology.

Because ground-based temperature networks are sparse or absent in most of the world's rapidly growing cities, satellite-derived land surface temperature (LST) has become the standard tool for characterizing the urban heat island at city scale. Thermal infrared sensors aboard the Landsat series of satellites, combined with a small set of normalized-difference spectral indices, allow researchers to reconstruct decades of urban thermal history from freely available imagery. The Normalized Difference Vegetation Index (NDVI), first formalized by Rouse, Haas, Schell and Deering (1974) for monitoring rangeland vegetation from early Earth Resources Technology Satellite data, remains the standard proxy for vegetation greenness in this literature. The Normalized Difference Built-up Index (NDBI), introduced by Zha, Gao and Ni (2003), plays an equivalent role for impervious and built-up surfaces, and the Modified Normalized Difference Water Index (MNDWI), proposed by Xu (2006), allows open water to be separated from both. Using these indices together with Landsat-derived LST, Weng, Lu and Schubring (2004) demonstrated in one of the most widely cited studies in this field that vegetation abundance and surface temperature are strongly and negatively related across an entire city, a finding that has since been replicated in dozens of cities on every inhabited continent.

South Asia, and Pakistan in particular, has urbanized rapidly over the past three decades, and its cities have increasingly become subjects of this literature. Mehmood, Zafar, Sajjad, Hussain, Zhai and Qin (2022) analyzed fifteen years of surface urban heat island intensity across six major cities of Punjab province using an autoregressive

Annual Methodological Archive Research Review
http://amresearchreview.com/index.php/Journal/about
Volume 3, Issue 10 (2025)

Online ISSN 3007-3197 Print ISSN 3007-3189
http://amresearchreview.com/index.php/Journal/about

time-series model and found statistically significant warming trends in most cities and seasons, with Gujranwala recording among the highest nighttime heat island intensities of the cities studied and a significant upward summer trend of 0.371 °C per year. Gujranwala itself, a densely built, industrially active city in central Punjab, has been the subject of more than one dedicated remote sensing study. Liaqut, Younes, Sadaf and Zafar (2018) reported that radiant surface temperature in the city rose by as much as eight degrees Celsius over roughly two decades of urban expansion and confirmed a negative relationship between NDVI and LST consistent with the wider literature. More recently, Ullah, Mehmood, Zhai and Qin (2025) combined Earth observation indices with machine-learning land cover classification to examine how land use and thermal conditions in Gujranwala have changed directionally and with distance from the city center between 2001 and 2021, projecting continued built-up expansion and vegetation loss toward 2041.

A separate and more recent strand of research asks whether the spatial arrangement of vegetation, not merely its total quantity, independently affects its cooling performance. Liu, Liu and Li (2024), studying landscape pattern effects on LST in Nanchang, China, found that for green land specifically, a more concentrated and contiguous patch structure, measured using the Largest Patch Index, was associated with lower surface temperature than an equal area of fragmented green land, while a higher number of separate patches was associated with warmer temperatures. Closer to the present study area, Khan and Li (2024) compared the landscape configuration effects of green space on LST in Beijing and Islamabad and found that, unlike in Beijing, patch density and related configuration metrics had a statistically significant influence on LST in Islamabad, suggesting that configuration effects documented elsewhere in the world may or may not generalize to South Asian, and specifically Pakistani, urban contexts.

Taken together, the existing literature on Gujranwala establishes that built-up land is warmer than vegetated land and that this differential has grown as the city has expanded, and the wider international literature on landscape configuration suggests, though with mixed results across cities, that the spatial arrangement of vegetation can modulate its cooling performance independently of its total amount. What has not yet been examined for Gujranwala, or for comparable rapidly urbanizing Pakistani cities more generally, is whether the efficiency of vegetation-associated cooling — that is, the amount of cooling delivered per unit of vegetation — varies systematically along a defined gradient from the urban core to the peri-urban periphery, and whether the spatial configuration of vegetation patches contributes explanatory power for surface temperature beyond what vegetation amount alone already provides. A conventional demonstration that more NDVI corresponds to lower LST in Gujranwala would add little to what is already established by prior work; the present study instead targets this more specific and less-studied combination of questions.

Based on this gap, the analysis is guided by three hypotheses: (H1) vegetation density is negatively associated with land surface temperature across the Gujranwala urban–peri-urban landscape; (H2) the magnitude of vegetation-associated surface cooling differs along the urban–peri-urban gradient; and (H3) larger and less fragmented vegetation patches are associated with greater local cooling than smaller and more fragmented patches of the same total vegetated area, after accounting for built-up

Annual Methodological Archive Research Review
http://amresearchreview.com/index.php/Journal/about
Volume 3, Issue 10 (2025)

Online ISSN 3007-3197 Print ISSN 3007-3189
http://amresearchreview.com/index.php/Journal/about

intensity.
Testing these hypotheses at city scale, across multiple decades, and at a spatial resolution fine enough to characterize individual patch configurations, is only practical using satellite remote sensing. Cloud-computing platforms for Earth observation, and open data products such as Landsat Collection 2 and the Dynamic World near-real-time land cover dataset (Brown et al., 2022), now make it possible to construct a decades-long, spatially detailed record of land surface temperature and vegetation structure for a single city without a dedicated field measurement campaign. The present study additionally applies statistical safeguards drawn from outside the remote sensing literature, specifically heteroskedasticity-robust regression standard errors following White (1980) and an explicit spatial sampling design intended to limit the inflated statistical significance that spatial autocorrelation can otherwise produce in gridded environmental data (Dormann et al., 2007), so that the associations reported below can be interpreted with appropriate statistical caution rather than treated as more certain than the underlying data support.
The specific objectives of this study are, first, to characterize the spatiotemporal evolution of land surface temperature and vegetation cover across Gujranwala between approximately 2000 and 2025 using a consistent, reproducible processing pipeline; second, to quantify the intensity of vegetation-associated cooling within four concentric distance zones extending from the urban core to fifteen kilometers into the peri-urban periphery, and to test whether this cooling intensity differs systematically across zones and epochs; and third, to evaluate, through a regression framework that controls for vegetation amount, elevation, distance from the core, and epoch, whether the spatial configuration of vegetation patches — specifically patch contiguity and patch density — provides additional explanatory power for surface temperature beyond vegetation amount alone.

Methodology

This section describes the study area, data sources, and processing pipeline used to test the hypotheses stated above. All satellite data processing was performed in Google Earth Engine; grid-level statistical analysis, patch-metric computation, and regression modeling were performed in Python. Figure 1 summarizes the overall workflow.

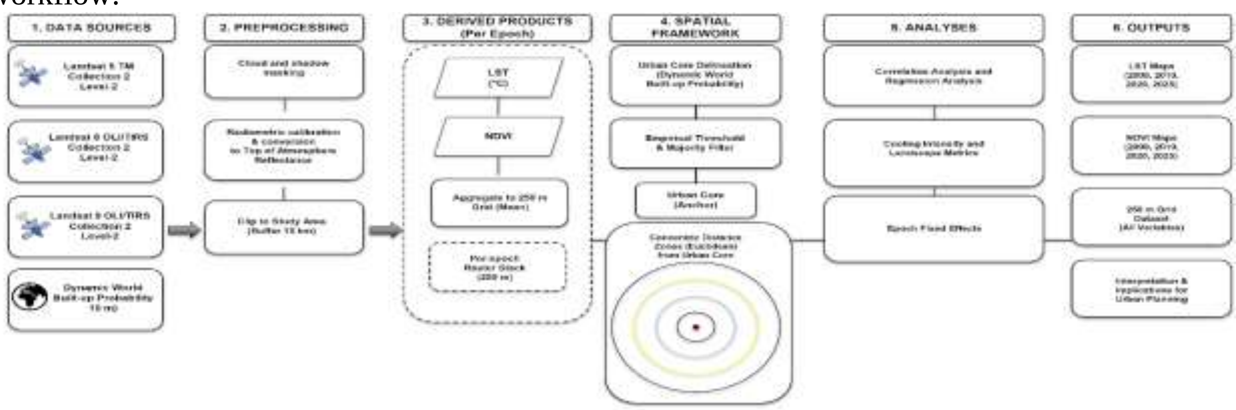

Figure 1. *Overview of the data processing and analysis workflow, from raw Landsat and Dynamic World inputs through spatial framework construction, grid-level*

Annual Methodological Archive Research Review
http://amresearchreview.com/index.php/Journal/about
Volume 3, Issue 10 (2025)

Online ISSN 3007-3197 Print ISSN 3007-3189
http://amresearchreview.com/index.php/Journal/about

analysis, and final outputs.

Study Area

Gujranwala is an important urban and agricultural region of northeastern Punjab, Pakistan, situated within the alluvial plains of the Upper Indus Basin at approximately 32.09° N and 74.19° E, with an elevation of about 226 m above sea level. The region forms part of the fertile alluvial landscape of the Rechna Doab and is influenced by the Chenab River system, with the wider Gujranwala–Sialkot region characterized by semi-arid to sub-humid monsoonal climatic conditions. Gujranwala has a strong agricultural base while simultaneously functioning as one of the major industrial and rapidly urbanizing centers of Punjab. Previous remote-sensing studies have documented substantial changes in land use/land cover associated with urban expansion, including the conversion of vegetated and agricultural surfaces to built-up land. The city has also experienced pronounced changes in land-surface thermal conditions associated with urban growth; remotely sensed analyses have reported higher surface temperatures over built-up areas compared with vegetated surfaces and an inverse relationship between vegetation abundance and land-surface temperature. The combination of productive agricultural land, expanding urban development, industrial activity, and increasing thermal pressure makes Gujranwala a suitable study area for investigating landscape transformation and its environmental implications using remote sensing and GIS. Agricultural activities are further linked with the region's groundwater resources, while studies in Gujranwala have highlighted the use of groundwater and, in some peri-urban areas, wastewater for crop irrigation.

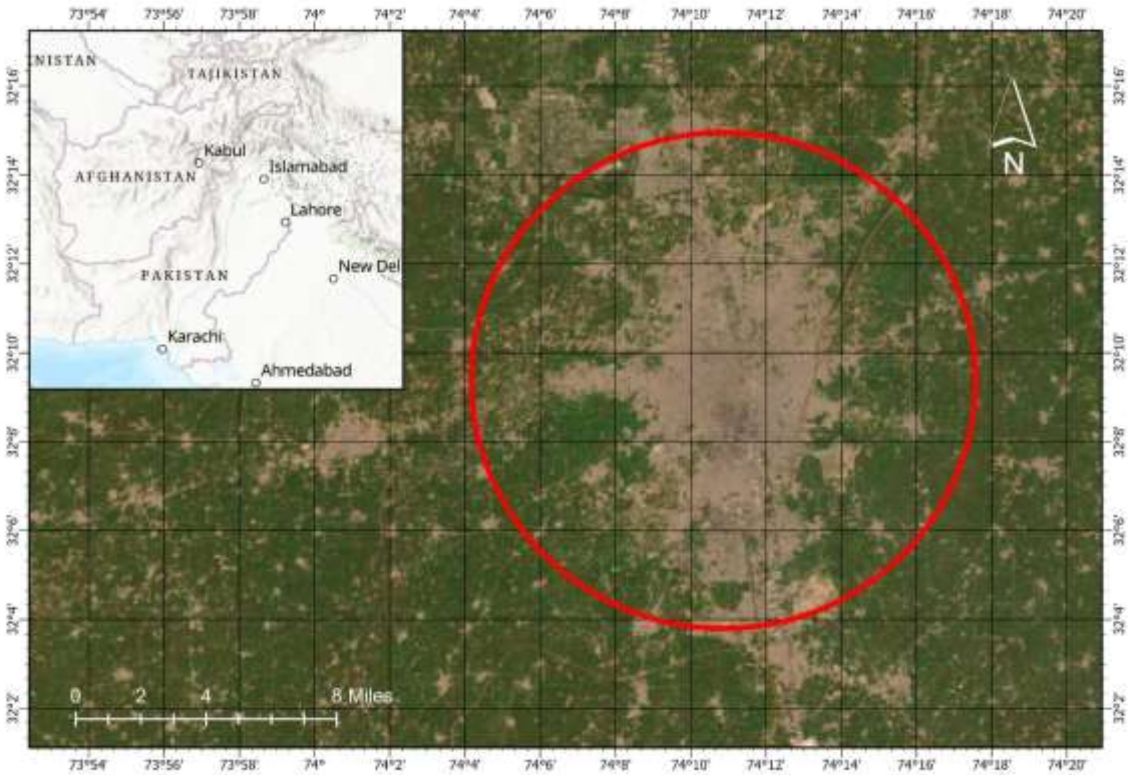

Figure 2. *Location of the Gujranwala study area within Punjab, Pakistan, with the*

Annual Methodological Archive Research Review
http://amresearchreview.com/index.php/Journal/about
Volume 3, Issue 10 (2025)

Online ISSN 3007-3197 Print ISSN 3007-3189
http://amresearchreview.com/index.php/Journal/about

15-kilometer study boundary shown in red.

Data Sources

Table 1 summarizes the datasets used, all of which are open access and were accessed through Google Earth Engine. Landsat Collection 2 Level-2 products supply atmospherically corrected surface reflectance together with a physically retrieved surface temperature band, so that LST did not need to be re-derived from raw thermal radiances. Dynamic World V1 (Brown et al., 2022), a near-real-time global land cover probability product derived from Sentinel-2 imagery using a deep learning classifier, was used solely to delineate the urban core boundary. The Copernicus GLO-30 digital elevation model provided a topographic control variable for the regression models.

Table 1. Datasets used in this study.

Dataset	Purpose	Resolution	Earth Engine source
FAO GAUL Level 2	Administrative boundary reference only	Vector	FAO/GAUL/2015/level2
Landsat 5 TM, Collection 2 Level 2	Surface reflectance and surface temperature, 2000 and 2010 epochs	30 m (thermal resampled)	LANDSAT/LT05/C02/T1_L2
Landsat 8 OLI/TIRS, Collection 2 Level 2	Surface reflectance and surface temperature, 2020 and 2025 epochs	30 m (thermal resampled)	LANDSAT/LC08/C02/T1_L2
Landsat 9 OLI-2/TIRS-2, Collection 2 Level 2	Surface reflectance and surface temperature, 2025 epoch, merged with Landsat 8	30 m (thermal resampled)	LANDSAT/LC09/C02/T1_L2
Dynamic World V1	Built-up probability for empirical urban core delineation	10 m	GOOGLE/DYNAMICWORLD/V1
Copernicus DEM GLO-30	Elevation control variable	30 m	COPERNICUS/DEM/GLO30

Urban Core Delineation and Distance-Zone Design

The urban core was delineated empirically rather than assumed from an arbitrary coordinate. Dynamic World built-up class probability was averaged over the 2024 calendar year within a twelve-kilometer search box centered on the approximate known location of Gujranwala city, a restriction intended to prevent other built-up settlements within the wider district from pulling the estimate away from the intended target. Pixels with a mean built probability exceeding 0.50 were classified as built-up;

Annual Methodological Archive Research Review
http://amresearchreview.com/index.php/Journal/about
Volume 3, Issue 10 (2025)

Online ISSN 3007-3197 Print ISSN 3007-3189
http://amresearchreview.com/index.php/Journal/about

this threshold was selected after comparing 0.40, 0.50, and 0.60 and confirming that 0.50 produced a total built-up area of 89.5 km², and an implied core radius of 5.34 km, consistent with the known extent of Gujranwala city. The urban core centroid was computed as the built-probability-weighted mean coordinate of these pixels, which converged on 32.165° N, 74.184° E, within approximately one kilometer of the city's commonly cited center. An equivalent-area circular core of radius 5.34 km was then used to define four concentric analysis zones extending outward from the core boundary: 0–2 km, 2–5 km, 5–10 km, and 10–15 km. The fifteen-kilometer outer boundary defines the full study area.

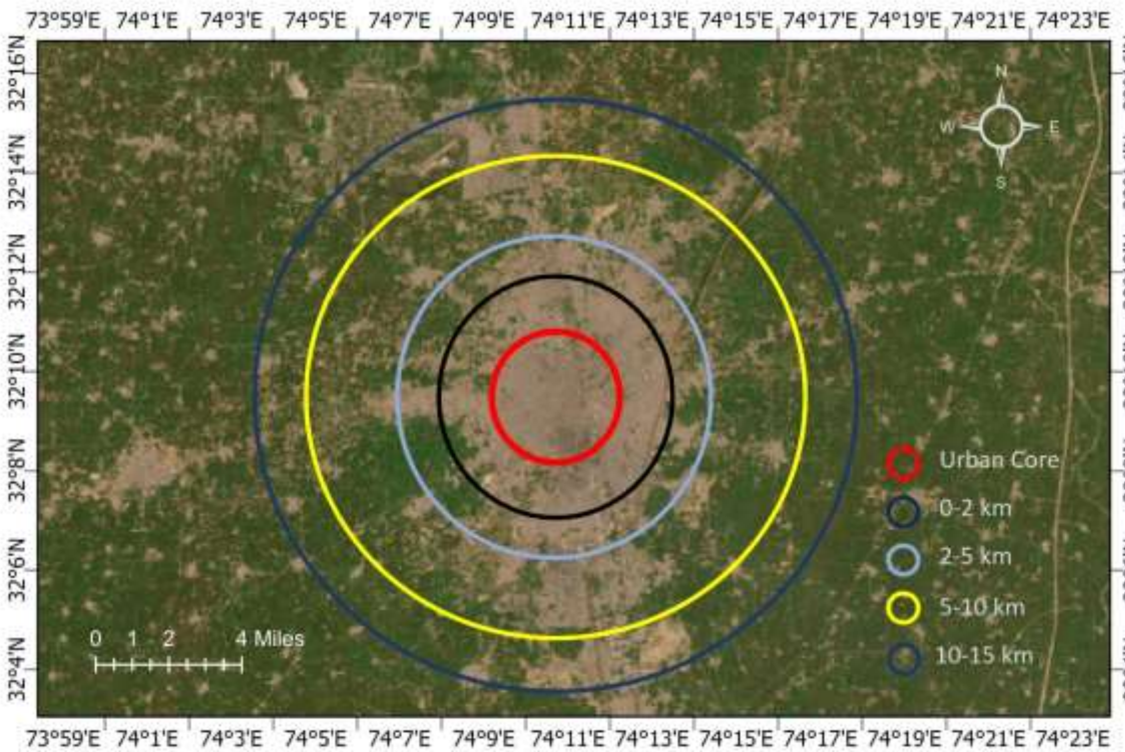

Figure 3. *The four concentric distance zones (0–2, 2–5, 5–10, and 10–15 kilometers from the urban core edge) used to characterize the urban–peri-urban gradient.*

An early implementation of the distance-from-core variable, computed in Earth Engine using a nearest-boundary-point distance function, was found on inspection to return increasing, rather than zero, distance values for locations deep inside the core polygon, because the function measures distance to the nearest boundary point rather than a signed inside–outside distance. This misclassified approximately one percent of grid cells (198 of 20,929) located near the exact geometric center of the study area into an incorrect outer zone. The error was identified during figure preparation and corrected by recomputing distance directly as the greater of zero and the Euclidean distance from each cell centroid to the core center, minus the core radius. All zone assignments, cooling metrics, and regression results reported in Section 3 use this corrected distance variable.

Online ISSN 3007-3197 Print ISSN 3007-3189

Temporal Design and Image Preprocessing

Four epochs were analyzed — approximately 2000, 2010, 2020, and 2025 — to provide a twenty-five-year perspective while keeping processing manageable. Because the Landsat 5 archive over Gujranwala contains few scenes in some years, the 2000 epoch was widened to a three-year window (1999–2001) to obtain an adequate sample of clear observations; the remaining three epochs each used a single calendar year. Within every epoch, only images acquired between April and June were retained. This pre-monsoon window was chosen after an initial data availability check found that the June–September window yielded too few cloud-free scenes for a reliable median composite (for example, only two clear scenes in 2000), whereas April–June consistently yielded more usable scenes with lower cloud contamination. Cloud, cloud shadow, and cirrus contamination were removed using the QA_PIXEL bitmask supplied with each Collection 2 scene, which implements the CFMask algorithm (Foga et al., 2017), itself an extension of the Fmask algorithm of Zhu, Wang and Woodcock (2015). Scenes with a metadata-reported cloud cover above 30 percent, or 40 percent for the sparser 2000 epoch, were excluded before compositing. A per-pixel median composite was then formed from the remaining cloud-masked scenes for each epoch, which further suppresses residual cloud and shadow contamination.

Surface reflectance and thermal bands were rescaled from digital numbers (DN) to physical units using the official Collection 2 scale factors. Reflectance (ρ) was obtained as:

$$\rho = 0.0000275 \times DN - 0.2 \quad (1)$$

and brightness temperature in kelvin (T) as:

$$T\,(K) = 0.00341802 \times DN + 149.0 \quad (2)$$

Land Surface Temperature Retrieval

LST was taken directly from the Collection 2 Level-2 surface temperature band rather than being re-derived from raw thermal radiances, consistent with the product's design as an analysis-ready, physically retrieved estimate. Kelvin values were converted to degrees Celsius as:

$$LST\,(°C) = T\,(K) - 273.15 \quad (3)$$

Before the resulting composites were used in any subsequent analysis, quality control was performed for each epoch by computing the minimum, fifth percentile, median, mean, ninety-fifth percentile, and maximum LST across the study area and visually inspecting the spatial pattern for values inconsistent with the region's known climate. All four epochs produced LST distributions within a physically plausible range for pre-monsoon Punjab, and no evidence of residual cloud contamination or masking artifacts was found.

Spectral Indices

Three normalized-difference indices were computed from each epoch's median composite. NDVI was calculated following Rouse et al. (1974) as:

$$NDVI = (NIR - Red) / (NIR + Red) \quad (4)$$

NDBI was calculated following Zha, Gao and Ni (2003) as:

$$NDBI = (SWIR - NIR) / (SWIR + NIR) \quad (5)$$

Online ISSN 3007-3197
Print ISSN 3007-3189
http://amresearchreview.com/index.php/Journal/about

and MNDWI was calculated following Xu (2006) as:

$$MNDWI = (Green - SWIR) / (Green + SWIR) \quad (6)$$

Band assignments were sensor-specific: for Landsat 5, green, red, near-infrared, and shortwave-infrared correspond to surface reflectance bands 2, 3, 4, and 5 respectively; for Landsat 8 and 9, to bands 3, 4, 5, and 6.

Water Masking and Data Quality Control

Water pixels, identified as MNDWI greater than 0.2, were excluded from all vegetation–temperature analyses to avoid contaminating cooling estimates with the distinct thermal behavior of open water. Grid cells with a missing value in any core analysis variable (LST, NDVI, NDBI, elevation, or distance from the core) after this masking were dropped listwise; this affected seven of 20,936 cells, a negligible fraction of the sample.

Spatial Sampling Design

Treating every thirty-meter pixel as an independent statistical observation would overstate the precision of any regression estimate, because both LST and vegetation cover are strongly spatially autocorrelated at short distances (Dormann et al., 2007). To address this, the study area was partitioned into a regular grid of 250 × 250 m cells in the UTM Zone 43N projection, yielding 20,929 valid cells per epoch and 83,716 cell-epoch observations in total across the four epochs. For each cell, the mean LST, NDVI, NDBI, elevation, and distance from the core were computed from the underlying thirty-meter pixels, and each cell was assigned to one of the four distance zones described above.

Cooling Intensity and Cooling Efficiency

For each vegetated grid cell (NDVI ≥ 0.2), a local Cooling Intensity (CI) was calculated as the mean LST of the most built-up cells (the top quartile of NDBI) within the same distance zone and epoch, minus the LST of the cell itself:

$$CI = LST(built, zone, epoch) - LST(cell) \quad (7)$$

Using a zone-and-epoch-specific built-up reference, rather than a single citywide value, ensures that Cooling Intensity reflects genuine local vegetation effects rather than a zone's overall baseline temperature. A Cooling Efficiency (CE) measure was additionally computed for cells with NDVI above 0.1, to avoid instability from dividing by values near zero:

$$CE = CI / NDVI \quad (8)$$

Because this normalized measure can behave erratically near its lower bound, it is treated in the Results as a secondary, exploratory measure rather than a primary one.

Vegetation Patch and Fragmentation Metrics

To test whether the spatial configuration of vegetation, independent of its total amount, is associated with LST, a binary vegetation mask (NDVI ≥ 0.3) was exported from Earth Engine as a thirty-meter raster for each of the four epochs. Landscape configuration metrics were then computed in Python using connected-component labeling with eight-neighbor connectivity, applied locally within each 250-meter grid cell rather than globally across the full raster. This choice matters: because

Online ISSN 3007-3197 Print ISSN 3007-3189
http://amresearchreview.com/index.php/Journal/about

agricultural fields in Gujranwala's peri-urban surroundings are frequently contiguous with one another, global connected-component labeling produces a small number of very large patches (in this raster, up to approximately 75 km²), which would be uninformative as a per-cell landscape statistic. Local, within-cell labeling instead captures genuine within-cell fragmentation. For each grid cell and epoch, the following metrics, consistent with the FRAGSTATS framework of McGarigal and Marks (1995), were computed: vegetated pixel fraction; number of local patches; mean and largest local patch size; the Largest Patch Index (the proportion of the cell's total vegetated area occupied by its single largest patch); patch density (patches per square kilometer); and edge density (meters of vegetation-to-non-vegetation boundary per unit cell area).

Statistical Models

All regression models used LST in degrees Celsius as the dependent variable, at the 250-meter grid-cell level, pooled across all four epochs ($n = 83{,}716$). Year was included as a categorical fixed effect in every model to absorb a systematic, epoch-level offset in mean LST that is described in Section 3.1 and is unrelated to the spatial relationships of interest; including this fixed effect ensures that comparisons by zone, by NDVI, and by patch configuration are made within each epoch rather than confounded by the between-epoch offset. Because ordinary least squares standard errors are invalid under heteroskedasticity, which is expected in a sample this large and spatially heterogeneous, all models were estimated with heteroskedasticity-consistent standard errors following White (1980). Three primary specifications were estimated: Model A, a vegetation-amount model (LST as a function of NDVI, elevation, distance from the core, and year); Model B, a built-up model (LST as a function of NDBI, elevation, distance, and year); and Model C, a fragmentation model testing H3 (LST as a function of NDVI, patch density, the Largest Patch Index, elevation, distance, and year). NDVI and NDBI were not included together in a single primary model because a variance inflation diagnostic confirmed strong collinearity between them (Pearson $r \approx -0.91$ in this dataset), which destabilizes and can reverse the sign of individual coefficients in a joint specification; a joint model was estimated only as an unreported robustness check. Model C's predictors returned acceptable variance inflation values, all below 1.5, indicating that vegetation amount and patch configuration provide sufficiently independent information for joint estimation.

Results

Data Availability and Quality Control

After restricting to the April–June pre-monsoon window and applying cloud cover and QA_PIXEL filtering, the number of Landsat scenes contributing to each epoch's median composite was fifteen for the approximately 2000 epoch (Landsat 5, widened to 1999–2001, cloud cover below 40 percent), fifteen for 2010 (Landsat 5, cloud cover below 30 percent), nine for 2020 (Landsat 8, cloud cover below 30 percent), and seventeen for 2025 (Landsat 8 and 9 combined, cloud cover below 30 percent). All four epochs produced LST distributions within a physically plausible range (Table 2), with no evidence of residual cloud or masking artifacts on visual inspection.

A systematic pattern in the pooled LST data has direct implications for how the

Annual Methodological Archive Research Review
http://amresearchreview.com/index.php/Journal/about
Volume 3, Issue 10 (2025)

Online ISSN 3007-3197
Print ISSN 3007-3189
http://amresearchreview.com/index.php/Journal/about

temporal results should be read. Mean LST alternated between comparatively cool epochs (36.55 °C in 2000 and 35.81 °C in 2020) and comparatively warm epochs (43.69 °C in 2010 and 42.53 °C in 2025), and this pattern held uniformly across all four distance zones (Table 3). Because this alternating pattern does not resemble a gradual, monotonic warming trend, and instead appears consistently across the entire study area regardless of zone, it most plausibly reflects a systematic difference in the precise within-season acquisition timing of the contributing scenes between epochs — for example, a later-June skew in 2010 and 2025 relative to an earlier-April skew in 2000 and 2020 — rather than a genuine year-over-year climate signal. Year was therefore included as a categorical fixed effect in every regression model (Section 2.11), so that all reported associations reflect within-epoch comparisons rather than this between-epoch offset. Raw differences in LST between epochs (for example, 2025 minus 2000) are accordingly not interpreted in this study as evidence of a twenty-five-year warming trend.

Spatial and Temporal Patterns of LST and NDVI

The mean LST ranged from 35.81 °C in 2020 to 43.69 °C in 2010, and mean NDVI ranged from 0.21 in 2010 to 0.35 in 2020 (Table 2).

Table 2. Descriptive statistics for land surface temperature, NDVI, and NDBI, pooled across the study area, by epoch.

Epoch	LST mean (°C)	LST SD	NDVI mean	NDVI SD	NDBI mean	NDBI SD
2000	36.55	1.47	0.22	0.06	0.00	0.04
2010	43.69	2.28	0.21	0.06	0.01	0.05
2020	35.81	2.41	0.35	0.10	− 0.06	0.07
2025	42.53	2.06	0.30	0.08	− 0.02	0.06

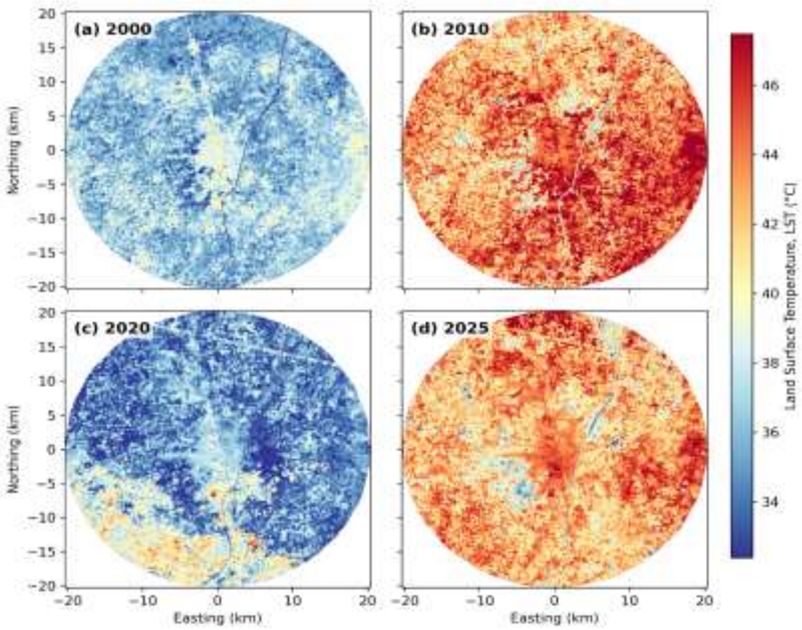

Annual Methodological Archive Research Review
http://amresearchreview.com/index.php/Journal/about
Volume 3, Issue 10 (2025)

Online ISSN 3007-3197 Print ISSN 3007-3189
http://amresearchreview.com/index.php/Journal/about

Figure 4. *Land surface temperature across all four epochs (2000, 2010, 2020, 2025), shown on a common color scale.*

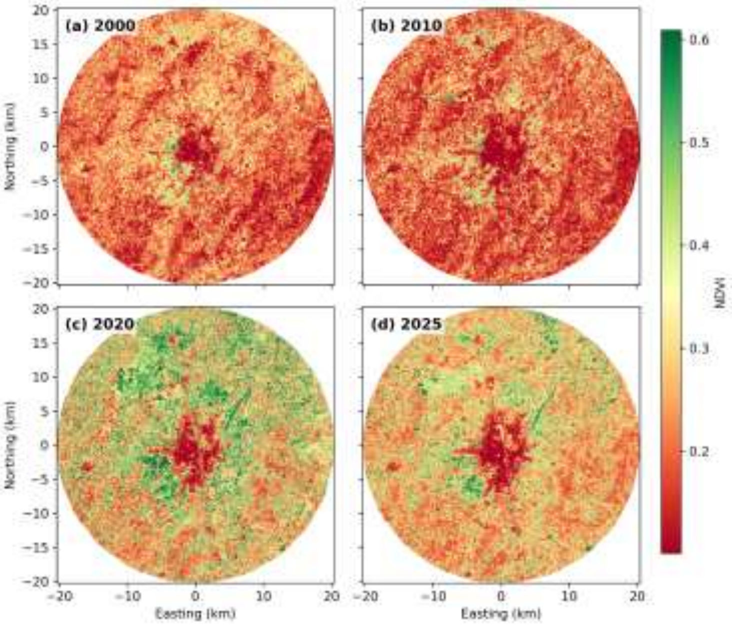

Figure 5. *NDVI across all four epochs (2000, 2010, 2020, 2025), shown on a common color scale.*

In every epoch, the urban core registered among the highest zone-mean LST values relative to the outer zones, although the size of this urban-core premium relative to the peri-urban zone was modest and varied by epoch, and was not consistent in every epoch (Table 3): the 0–2 km zone was 0.18 °C warmer than the 10–15 km zone in 2000, while in 2020 the core was marginally cooler, by 0.33 °C, than the peri-urban zone, and in 2025 the core was likewise 0.48 °C cooler than the peri-urban zone. This zone-level variability motivated the cooling-intensity analysis described next, which controls for each zone's local built-up baseline rather than relying on a simple core-versus-periphery comparison of raw LST.

Table 3. Mean land surface temperature (°C) by distance zone and epoch.

Zone	2000	2010	2020	2025
0–2 km (core)	36.67	44.07	35.79	42.28
2–5 km	36.45	43.72	35.11	41.82
5–10 km	36.63	43.58	35.67	42.61
10–15 km	36.48	43.64	36.11	42.76

The Vegetation–Temperature Relationship

Consistent with the wider literature reviewed in the Introduction, NDVI and LST were strongly and negatively related across the pooled dataset. Grid cells classified into sparse (NDVI < 0.2), low-to-moderate (0.2–0.4), moderate-to-high (0.4–0.6), and dense (> 0.6) vegetation classes showed a clear, monotonic decline in mean LST from the sparsest to the densest class, from approximately 44.5 °C for sparse vegetation to approximately 35.3 °C for dense vegetation in the 2025 epoch — a spread of roughly

Annual Methodological Archive Research Review
http://amresearchreview.com/index.php/Journal/about
Volume 3, Issue 10 (2025)

Online ISSN 3007-3197 Print ISSN 3007-3189
http://amresearchreview.com/index.php/Journal/about

nine degrees.

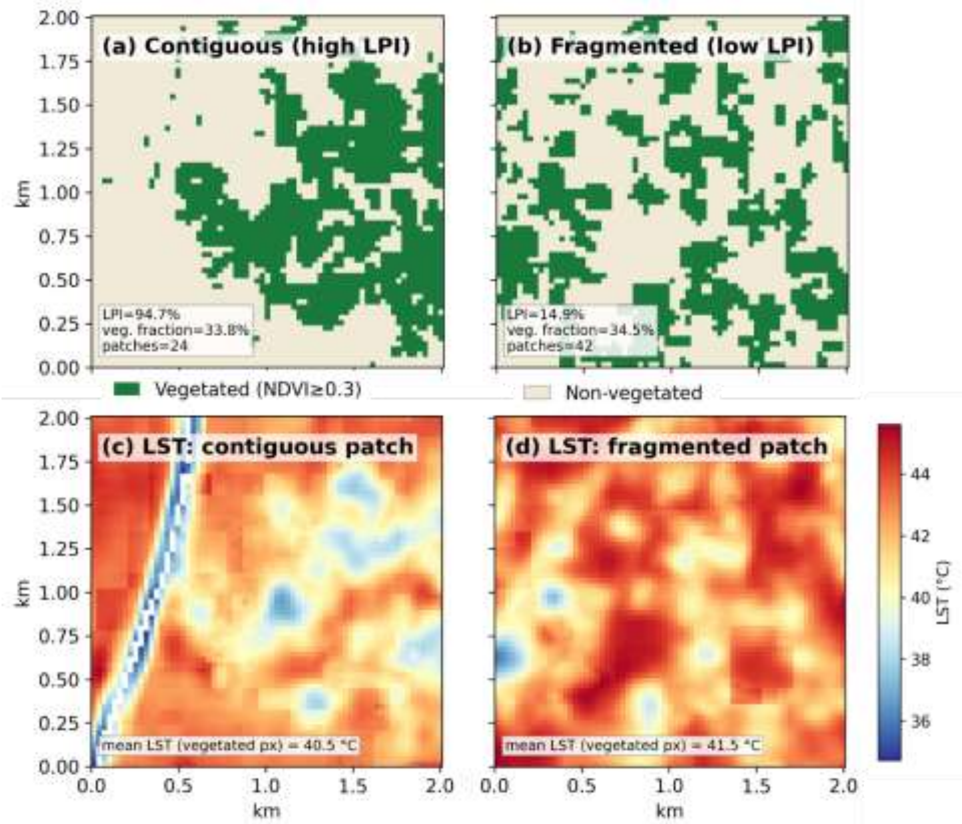

Figure 6. *(a) NDVI plotted against LST, colored by distance zone, for a representative sample of grid cells. (b) The Largest Patch Index plotted against LST, colored by distance zone, for the same sample.*

In the vegetation-amount model (Model A: LST as a function of NDVI, elevation, distance, and year; heteroskedasticity-robust standard errors; n = 83,716; $R^2 = 0.835$), the NDVI coefficient was − 16.54 (SE 0.084, $p < 0.001$): holding elevation, distance from the core, and epoch constant, a one-unit increase in NDVI was associated with a 16.54 °C decrease in LST. In the built-up model (Model B: LST as a function of NDBI, elevation, distance, and year; $R^2 = 0.871$), the NDBI coefficient was + 27.50 (SE 0.104, $p < 0.001$), confirming the expected positive association between built-up density and surface temperature (Table 4). NDVI and NDBI were not combined in a single primary model because of their strong negative correlation ($r \approx -0.91$ in this dataset); a joint specification was estimated only as a robustness check and, as expected under collinearity, produced an unstable, sign-reversed NDVI coefficient, which is why the vegetation-amount and built-up models are reported separately as the primary results.

Cooling Intensity Along the Urban–Peri-Urban Gradient

Cooling Intensity — the local built-up reference LST minus the vegetated-cell LST within the same zone and epoch — followed a broadly consistent pattern in three of the four epochs: the urban core and inner-urban zones showed higher mean cooling intensity than the outer fringe and peri-urban zones (Table 5). In 2000, the core's

Online ISSN 3007-3197 Print ISSN 3007-3189
http://amresearchreview.com/index.php/Journal/about

mean Cooling Intensity was 2.66 °C, compared with 1.98 °C in the peri-urban zone; in 2010, 3.62 °C compared with 3.05 °C; and in 2025, 2.90 °C compared with 1.93 °C. The exception was 2020, in which the peri-urban zone (2.56 °C) modestly exceeded the core (2.33 °C). Overall, in three of the four analyzed epochs, vegetation located closer to the urban core delivered more cooling, relative to the local built-up temperature baseline, than vegetation in the outer peri-urban zone, a pattern consistent with H2, while the exception in 2020 indicates that the relationship is not perfectly monotonic in every epoch and zone.

Table 5. Mean Cooling Intensity (°C) by distance zone and epoch, for vegetated cells (NDVI ≥ 0.2).

Zone	**2000**	**2010**	**2020**	**2025**
0–2 km (core)	2.66	3.62	2.33	2.90
2–5 km	1.81	3.22	1.62	2.13
5–10 km	1.64	2.47	2.00	1.72
10–15 km	1.98	3.05	2.56	1.93

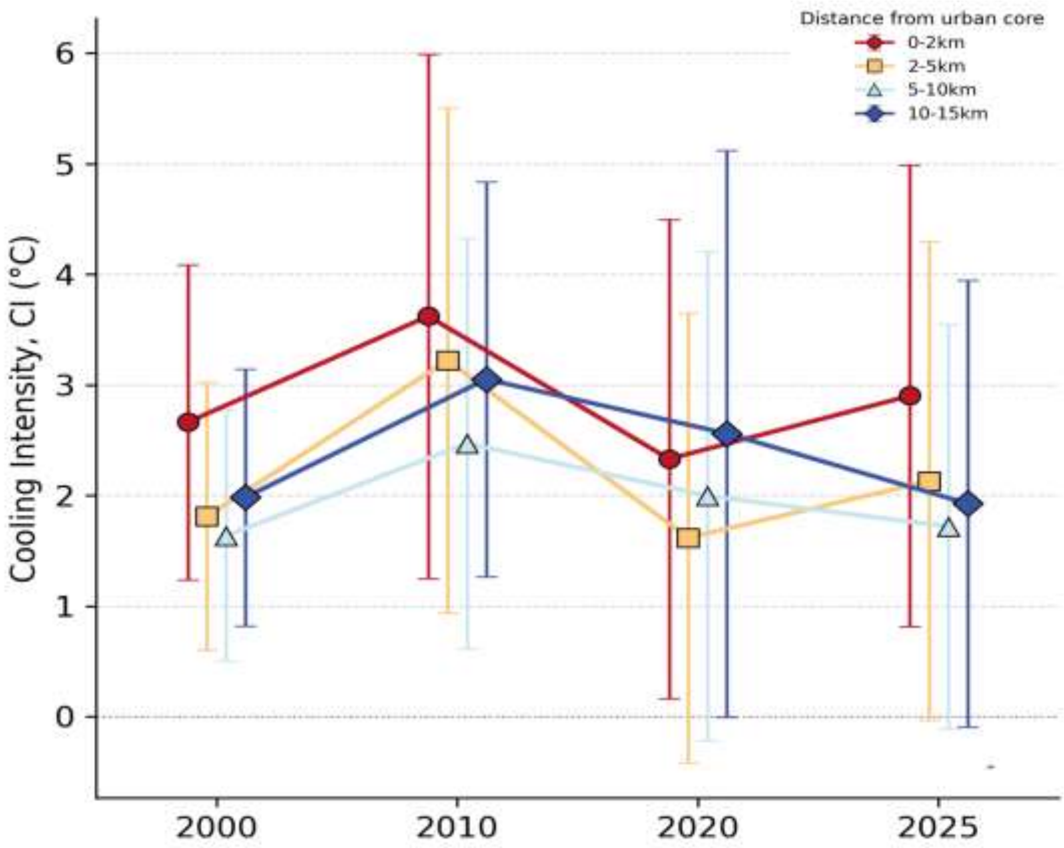

Figure 7. *Cooling Intensity by distance zone across the four study epochs (2000, 2010, 2020, 2025).*

Cooling Efficiency (Cooling Intensity normalized by NDVI) followed a broadly similar but noisier pattern across zones and epochs. Because this normalized measure can behave unstably as NDVI approaches its lower bound, it is reported here only as a

Annual Methodological Archive Research Review
http://amresearchreview.com/index.php/Journal/about
Volume 3, Issue 10 (2025)

Online ISSN 3007-3197 Print ISSN 3007-3189

http://amresearchreview.com/index.php/Journal/about

secondary, exploratory result rather than a primary finding.

Regression Models

Table 4. Regression coefficients (heteroskedasticity-robust standard errors in parentheses) for the three primary LST models. All models include year fixed effects. *** $p < 0.001$.

Variable	Model A (vegetation)	Model B (built-up)	Model C (fragmentation)
NDVI	− 16.543*** (0.084)	—	− 16.069*** (0.098)
NDBI	—	27.504*** (0.104)	—
Patch density (per km²)	—	—	− 0.0049*** (0.0003)
Largest Patch Index	—	—	− 0.156*** (0.020)
Elevation (m)	− 0.007*** (0.001)	− 0.018*** (0.001)	− 0.007*** (0.001)
Distance from core (m)	1.45×10^{-5}*** (1.27×10^{-6})	− 2.73×10^{-5}*** (1.15×10^{-6})	1.46×10^{-5}*** (1.26×10^{-6})
R^2	0.8346	0.8709	0.8352
N (observations)	83,716	83,716	83,716

Green-Space Configuration and Fragmentation

The fragmentation model (Model C: LST as a function of NDVI, patch density, the Largest Patch Index, elevation, distance, and year; $R^2 = 0.835$) tested whether vegetation configuration provides explanatory power for LST beyond vegetation amount alone. Both configuration predictors were statistically significant. The Largest Patch Index coefficient was − 0.156 (SE 0.020, $p < 0.001$): holding vegetation amount and the other covariates constant, grid cells whose vegetated area was concentrated into a single dominant contiguous patch registered lower LST, consistent with H3 and with the direction reported for green land in Nanchang by Liu, Liu and Li (2024). Patch density, however, returned a coefficient of − 0.0049 (SE 0.0003, $p < 0.001$), a small but statistically significant association in which a greater number of local patches was associated with lower, not higher, LST once NDVI and the Largest Patch Index were held constant. This direction runs counter to the intuitive expectation that fragmentation should uniformly impair cooling, and it does not match the positive patch-density and land-surface-temperature relationship that Khan and Li (2024) reported specifically for Islamabad.

The practical contribution of adding these configuration variables to the model was small: R^2 increased from 0.8346 in the vegetation-amount model to 0.8352 in the fragmentation model, an increase of approximately 0.06 percentage points. Given the very large sample size, even a small true effect will register as statistically significant, so this result is best read as evidence that vegetation amount remains the dominant predictor of surface temperature in this study area, while vegetation configuration contributes a real but modest, and directionally mixed, additional signal. This is interpreted as partial, cautious support for H3: patch contiguity is associated with cooling in the theoretically expected direction, while patch count is not, and neither configuration metric approaches vegetation amount in explanatory importance.

Annual Methodological Archive Research Review
http://amresearchreview.com/index.php/Journal/about
Volume 3, Issue 10 (2025)

Online ISSN 3007-3197 Print ISSN 3007-3189
http://amresearchreview.com/index.php/Journal/about

Discussion

The results confirm, across a large and spatially systematic sample, a relationship documented in a wide range of urban settings: land surface temperature declines as vegetation cover increases and rises as built-up density increases. The magnitude of the NDVI effect found here — a coefficient of roughly − 16.5 °C per unit increase in NDVI — sits within the range reported by Weng, Lu and Schubring (2004) for Indianapolis and is directionally consistent with the vegetation-cooling relationship documented specifically for Gujranwala by Liaqut, Younes, Sadaf and Zafar (2018) and, at a province-wide scale that included Gujranwala, by Mehmood et al. (2022). What this study adds is not a demonstration that vegetation cools Gujranwala, which prior work has already established, but a more specific test of where that cooling is strongest and whether its spatial delivery depends on how the vegetation is arranged — a question that sits at the intersection of urban climatology and landscape ecology rather than within either field alone.

The zone-level cooling intensity results offer qualified support for the hypothesis that cooling effectiveness varies along the urban–peri-urban gradient. In three of the four epochs, vegetation in the urban core and inner-urban zones delivered more cooling relative to the local built-up baseline than vegetation in the outer fringe and peri-urban zones. This pattern is consistent with the general logic of park-cooling-intensity research, in which the size of the temperature contrast a green patch produces depends partly on how thermally stressed its surroundings already are, so the same amount of vegetation embedded in a hotter built matrix generates a larger relative contrast than it would in an already cooler, more vegetated periphery. The 2020 exception, in which the peri-urban zone showed marginally higher cooling intensity than the core, is not fully explained by the available data. It coincides with the smallest number of contributing Landsat 8 scenes of any epoch (nine, against fifteen to seventeen elsewhere) and may reflect either that reduced sample or genuine but undocumented land-management change at the fringe during that period. This is a reason for caution in that specific epoch rather than grounds to reject the gradient pattern found in the other three.

The fragmentation results are the most novel part of this study and benefit from being read through the lens of landscape ecology rather than remote sensing alone. Two long-standing ecological findings help explain why patch contiguity, and not just patch quantity, should matter for microclimate. First, the classic edge-microclimate work of Chen, Franklin and Spies (1995), conducted in forest clearcut systems but broadly applicable to any vegetation-matrix boundary, showed that air temperature, radiation, and humidity all form measurable gradients from a patch edge into its interior, with edge influence typically extending from roughly 30 to more than 200 meters depending on the variable and conditions. A patch small enough, or irregular enough, to be entirely within this edge-influence zone has, in effect, no true thermal interior: every part of it is coupled to the surrounding matrix's temperature regime. A single large contiguous patch, by contrast, retains a buffered core that is only partially influenced by the surrounding built environment. This is a plausible mechanistic explanation for why the Largest Patch Index, which measures exactly this contiguity, was associated with lower LST in this study, consistent with the equivalent finding for green land in Nanchang reported by Liu, Liu and Li (2024). Second, Forman's (1995)

Annual Methodological Archive Research Review
http://amresearchreview.com/index.php/Journal/about
Volume 3, Issue 10 (2025)

Online ISSN 3007-3197 Print ISSN 3007-3189
http://amresearchreview.com/index.php/Journal/about

patch-corridor-matrix framework, one of the foundational conceptual models in landscape ecology, treats the surrounding matrix — in this case, the built environment — as an active determinant of patch behavior rather than a passive background; a patch's ecological and microclimatic performance depends on the matrix it sits within as much as on the patch itself. This framework is useful for interpreting why the same vegetation configuration metric can behave differently in different settings: in Gujranwala's peri-urban periphery, where the matrix is itself largely agricultural vegetation rather than impervious surface, the edge-effect logic that governs a park surrounded by pavement does not straightforwardly apply, which is also why patch metrics were computed locally within each 250-meter cell in this study rather than globally, to avoid conflating a genuinely different matrix context with the city's built core.

This same reasoning helps situate the patch-density result, which did not align with the positive patch-density and LST relationship that Khan and Li (2024) reported specifically for Islamabad. Khan and Li computed configuration metrics using a one-square-kilometer moving window centered on a single city's formal park system, whereas the present study computed metrics within much smaller 250-meter cells pooled across an entire gradient that includes large expanses of contiguous peri-urban farmland with no clear analogue in Islamabad's green-space inventory. Given the edge-depth findings of Chen et al. (1995), a metric like patch density, which counts patches without regard to their size or the matrix surrounding them, is likely to behave inconsistently across studies that differ in analysis window size and matrix composition, and this inconsistency across two Pakistani cities is itself informative: it suggests that patch density is a less stable indicator of cooling performance than patch contiguity, which behaved consistently with theoretical expectations in both this study and the Nanchang case. In either case, the small overall gain in explanatory power from adding configuration metrics to the vegetation-amount model — an increase in R^2 of about 0.06 percentage points — indicates that whatever contribution patch configuration makes to surface cooling in Gujranwala is secondary to the contribution of vegetation amount itself. A further ecological caveat is that NDVI, the amount measure used throughout this study, does not distinguish vegetation structure or type; canopy trees, shrubs, and irrigated lawns can register similar NDVI values while differing substantially in transpiration rate and shading depth, a distinction Weng, Lu and Schubring (2004) also raised in comparing NDVI to sub-pixel fractional vegetation cover. This study cannot separate a true configuration effect from an unmeasured difference in vegetation type that happens to correlate with patch shape, and this is a limitation rather than a settled finding.

Several further limitations should be stated plainly. The four analysis epochs were not acquired under matched within-season conditions: 2010 and 2025 registered systematically warmer composite LST than 2000 and 2020 across every distance zone, most consistent with differences in the precise day-of-year composition of the contributing Landsat scenes rather than genuine inter-annual warming. Year fixed effects address this at the level of statistical inference but cannot recover a true multi-decadal trend, and none is claimed here. This is an observational, cross-sectional analysis at each epoch, so none of the associations reported should be read as demonstrating causation, only robust association after accounting for elevation,

Annual Methodological Archive Research Review
http://amresearchreview.com/index.php/Journal/about
Volume 3, Issue 10 (2025)
Online ISSN 3007-3197 Print ISSN 3007-3189
http://amresearchreview.com/index.php/Journal/about

distance from the core, and epoch. The native thermal-band resolution of the Landsat sensors used, on the order of 100 m before Collection 2 resampling, is coarser than the 30-meter vegetation mask used for patch metrics, a mismatch that may partly explain why configuration effects were detectable but small, since fine patch boundaries may not be fully resolved in the underlying thermal signal, a concern directly related to the edge-depth scales documented by Chen et al. (1995). The urban core boundary depends on a built-up probability threshold selected through sensitivity testing rather than derived independently, and water masking relied on a single MNDWI threshold rather than a validated water product.

These limitations point toward specific next steps rather than undermining the core findings. Reconstructing the four epochs within a narrower, matched day-of-year window would isolate genuine inter-annual change from within-season acquisition variability. Incorporating vegetation structure data, such as canopy height or a tree-versus-grass classification, alongside NDVI would help separate a true patch-configuration effect from a confounded vegetation-type effect, directly addressing the ecological caveat raised above. Finally, replicating this gradient-and-configuration design in other rapidly urbanizing Pakistani cities, ideally using a consistent analysis window size chosen with reference to documented edge-influence depths rather than an arbitrary grid resolution, would help establish whether the patterns found here are specific to Gujranwala or reflect a more general feature of vegetation–temperature relationships in South Asian urban–peri-urban landscapes.

Conclusion

This study assessed how vegetation-associated cooling varies across the urban–peri-urban gradient of Gujranwala, Pakistan, and whether the spatial configuration of vegetation patches, not just their total amount, helps explain land surface temperature. Using Landsat 5, 8, and 9 imagery processed in Google Earth Engine across four epochs between 2000 and 2025, aggregated to a 250-meter grid of 83,716 cell-epoch observations, the analysis confirmed a strong negative NDVI–LST relationship and a strong positive NDBI–LST relationship, consistent with prior Gujranwala-specific and international literature. Cooling intensity, calculated relative to a local built-up reference temperature, was generally higher in the urban core and inner-urban zones than in the outer fringe and periphery, supporting the hypothesis that cooling effectiveness varies with position along the gradient, though not in every epoch examined. Vegetation patch configuration added only a small amount of explanatory power beyond vegetation amount: patch contiguity, measured by the Largest Patch Index, was associated with cooling in the direction predicted by landscape-ecological theory and consistent with comparable findings from Nanchang, while patch density showed the opposite sign to a comparable Islamabad study, a discrepancy plausibly linked to differences in analysis scale and surrounding matrix composition. A systematic offset in mean LST between epochs, most likely driven by within-season acquisition-date differences rather than genuine warming, was identified and controlled for statistically rather than over-interpreted as a climate trend. Overall, the study indicates that in Gujranwala, the amount of vegetation present remains the primary determinant of surface cooling, while its spatial arrangement contributes a real but modest and only partially consistent secondary effect — a nuanced

Online ISSN 3007-3197
Print ISSN 3007-3189
http://amresearchreview.com/index.php/Journal/about

conclusion that is itself a meaningful contribution given that no prior study of this city had tested the configuration question directly. These findings suggest that urban greening policy in Gujranwala would gain more from increasing the overall extent of vegetation, particularly within the urban core where its relative cooling contrast is greatest, than from prioritizing patch shape alone, while also indicating that consolidating new green space into larger, more contiguous patches, where feasible, is likely to modestly outperform an equal area of scattered smaller plantings.

Author Contributions

Conceptualization: Nouman Akhtar; Methodology, Data curation, and Formal analysis: Basit Aziz; Visualization: Zeeshan Haider; Review & Editing: Razi ur Rehman.

Conflicts of Interest

The authors declare that they have no competing interests.

References

Brown, C. F., Brumby, S. P., Guzder-Williams, B., Birch, T., Hyde, S. B., Mazzariello, J., Czerwinski, W., Pasquarella, V. J., Haertel, R., Ilyushchenko, S., et al. (2022). Dynamic World, near real-time global 10 m land use land cover mapping. *Scientific Data*, *9*, 251. https://doi.org/10.1038/s41597-022-01307-4

Chen, J., Franklin, J. F., & Spies, T. A. (1995). Growing-season microclimatic gradients from clearcut edges into old-growth Douglas-fir forests. *Ecological Applications*, *5*(1), 74–86.

Dormann, C. F., McPherson, J. M., Araújo, M. B., Bivand, R., Bolliger, J., Carl, G., Davies, R. G., Hirzel, A., Jetz, W., Kissling, W. D., Kühn, I., Ohlemüller, R., Peres-Neto, P. R., Reineking, B., Schröder, B., Schurr, F. M., & Wilson, R. (2007). Methods to account for spatial autocorrelation in the analysis of species distributional data: A review. *Ecography*, *30*(5), 609–628. https://doi.org/10.1111/j.2007.0906-7590.05171.x

Foga, S., Scaramuzza, P. L., Guo, S., Zhu, Z., Dilley, R. D., Beckmann, T., Schmidt, G. L., Dwyer, J. L., Hughes, M. J., & Laue, B. (2017). Cloud detection algorithm comparison and validation for operational Landsat data products. *Remote Sensing of Environment*, *194*, 379–390. https://doi.org/10.1016/j.rse.2017.03.026

Forman, R. T. T. (1995). *Land mosaics: The ecology of landscapes and regions.* Cambridge University Press.

Haroon, M., Al-Saadi, A. A., & Iqbal, M. A. (2021). Comparative exposure assessment of potential health risks through the consumption of vegetables irrigated by freshwater/wastewater: Gujranwala, Pakistan. *Chemical Research in Toxicology*, *34*(6), 1417–1429. https://doi.org/10.1021/acs.chemrestox.0c00277

Khan, M. S., & Li, Y. (2024). Comparative study and effects of urban green scape on the land surface temperature of a large metropolis and green city. *Heliyon*, *10*(3), e24912. https://doi.org/10.1016/j.heliyon.2024.e24912

Online ISSN 3007-3197 Print ISSN 3007-3189
http://amresearchreview.com/index.php/Journal/about

Liaqut, A., Younes, I., Sadaf, R., & Zafar, H. (2018). Impact of urbanization growth on land surface temperature using remote sensing and GIS: A case study of Gujranwala City, Punjab, Pakistan. *International Journal of Economic and Environmental Geology*, *9*(3), 44–49. https://doi.org/10.46660/ijeeg.v9i3.735

Liu, P., Liu, C., & Li, Q. (2024). Effects of landscape pattern on land surface temperature in Nanchang, China. *Scientific Reports*, *14*, 3832. https://doi.org/10.1038/s41598-024-54046-4

McGarigal, K., & Marks, B. J. (1995). *FRAGSTATS: Spatial pattern analysis program for quantifying landscape structure* (General Technical Report PNW-GTR-351). USDA Forest Service, Pacific Northwest Research Station. https://doi.org/10.2737/PNW-GTR-351

Mehmood, H. (2022). Spatio-temporal trends and patterns of urban sprawl in Gujranwala City, Punjab–Pakistan. *Pakistan Journal of Science.*

Mehmood, M. S., Zafar, Z., Sajjad, M., Hussain, S., Zhai, S., & Qin, Y. (2022). Time series analyses and forecasting of surface urban heat island intensity using ARIMA model in Punjab, Pakistan. *Land*, *12*(1), 142. https://doi.org/10.3390/land12010142

Nadeem, F., Jacobs, B., & Cordell, D. (2022). Mapping agricultural vulnerability to impacts of climate events of Punjab, Pakistan. *Regional Environmental Change*, *22*, 66. https://doi.org/10.1007/s10113-022-01918-y

Rouse, J. W., Haas, R. H., Schell, J. A., & Deering, D. W. (1974). Monitoring vegetation systems in the Great Plains with ERTS. In *Third Earth Resources Technology Satellite-1 Symposium* (NASA SP-351, pp. 309–317). NASA.

Tahir, F., Mirza, A. I., Sarwar, M., & Mahmood, S. (2025). Spatial analysis of land use and land cover of Gujranwala District using remotely sensed data. *International Journal of Innovations in Science & Technology*, *7*(Special Issue), 258–265. https://doi.org/10.33411/IJIST/1509

Ullah, Z., Mehmood, M. S., Zhai, S., & Qin, Y. (2025). Analysis of LULC and urban thermal variations in industrial cities using earth observation indices and machine learning: A case study of Gujranwala, Pakistan. *Remote Sensing*, *17*(14), 2474. https://doi.org/10.3390/rs17142474

Weng, Q., Lu, D., & Schubring, J. (2004). Estimation of land surface temperature–vegetation abundance relationship for urban heat island studies. *Remote Sensing of Environment*, *89*(4), 467–483. https://doi.org/10.1016/j.rse.2003.11.005

White, H. (1980). A heteroskedasticity-consistent covariance matrix estimator and a direct test for heteroskedasticity. *Econometrica*, *48*(4), 817–838. https://doi.org/10.2307/1912934

Xu, H. (2006). Modification of normalised difference water index (NDWI) to enhance open water features in remotely sensed imagery. *International Journal of Remote Sensing*, *27*(14), 3025–3033. https://doi.org/10.1080/01431160600589179

Zha, Y., Gao, J., & Ni, S. (2003). Use of normalized difference built-up index in automatically mapping urban areas from TM imagery. *International Journal of Remote Sensing*, *24*(3), 583–594. https://doi.org/10.1080/01431160304987

Zhu, Z., Wang, S., & Woodcock, C. E. (2015). Improvement and expansion of the

Online ISSN 3007-3197
Print ISSN 3007-3189
http://amresearchreview.com/index.php/Journal/about

Fmask algorithm: Cloud, cloud shadow, and snow detection for Landsats 4–7, 8, and Sentinel 2 images. *Remote Sensing of Environment*, *159*, 269–277. https://doi.org/10.1016/j.rse.2014.12.014